Virtual Flattening of Clothing Item Held in the Air

Yasuyo Kita and Nobuyuki Kita
Intelligent Systems Research Institute
National Institute of Advanced Industrial Science and Technology
AIST Tsukuba Central 1, 1-1-1 Umezono, Tsukuba, Ibaraki 305-8560, Japan
Email: y.kita{n.kita}@aist.go.jp

Abstract—We propose a method of virtually flattening the surface of a clothing item to a two-dimensional plane using the geodesic distance over the surface of the item. If a clothing item is flatly opened on a table, the recognition of the item is much easier than that of the same item having an arbitrary shape. However, it is difficult and troublesome to physically flatten a clothing item from its arbitrary shape automatically. We therefore propose to develop the surface of the clothing item held in the air into a two-dimensional shape using three-dimensional observation data of the surface. To this end, boundary points of the observed clothing region are sampled as start/end nodes for calculating geodesic lines, the lengths of which become two-dimensional distances between the points when the surface is flattened to a plane. To robustly calculate geodesic lines using a three-dimensional point cloud of the surface, we adopt a method that interpolates the depth and normal direction at any point on the surface using the element-free Galerkin method. The shortest path along the surface between two points on the surface is then calculated using these depths and normal directions in the framework of the "zero-length spring analogy". The two-dimensional coordinates of the points on the plane are obtained by solving simultaneous equations determined by the geodesic distances. We also propose a method of using the flattened view for the classification of clothing type and detection of important parts of clothing. Preliminary experiments using long-sleeve shirts and trousers as clothing items demonstrate the promise of the proposed methods.

I. Introduction

Home and rehabilitation robots are expected to play an important role in an aging society and it will become necessary for robots to automatically handle daily objects including clothing items. The large deformation of clothing items that is accompanied by complex self-occlusion makes the task of recognizing items challenging. A model-driven approach works well when the geometrical model of the item of interest is known in advance [1][2]. However, without this previous knowledge, the problem is more difficult owing to the tremendous variation in clothing shapes.

Most studies on the subject have tried to first spread the clothing item using a fixed sequence of actions. Osawa et al. [3] proposed a method that re-grasps the lowest point of a clothing item twice to reduce the deformation variation. However, the shapes that form after the actions are not necessarily discriminating and there is often undesired twisting of the item. Hue et al.[4] proposed a method of finding the appropriate grasping point for opening an item into a small number of limited shapes from a sequence of three-dimensional (3D) data obtained from various viewing

directions. However, the success rate of opening in their experiments was not enough high. Triantafyllou et al. [5] proposed a method of flattening clothing items while allowing half-folded shapes and matched the flattened item with a foldable template. However, it remains difficult to robustly bring clothing into such flat shapes with only one fold.

Doumanoglou et al. [6] used 3D features extracted from depth images of clothing items to classify the clothing category and to detect the position to hold according to the random forests algorithm. Although they obtained good results even for items different from those used in the learning stage, their methods require approximately 30,000 observation data for training to achieve good results. It is uncertain if the learned classifier still works when the situation (i.e., the robotics and 3D sensors) changes.

If the material of the clothing item is relatively thick, the shape of the item when the item is held by one hand is sufficiently informative to tell the clothing type and size. In fact, a human can imagine the flattened shape from a three-dimensionally deformed shape. Our aim is to realize this "virtual flattening" function by transforming the 3D surface into a two-dimensional (2D) shape. Hereafter, we refer to the shape after virtual flattening as the flattened view. In this paper, by limiting ourselves to the case that most of one side of a clothing item that is held in the air can be observed from one direction, we propose a fundamental method for virtually flattening the clothing surface on a plane using the geodesic distance of the surface. Although our previous paper [7] also used geodesic distances in estimating the flattened view, that method approximates the geodesic lines with the contours of horizontal cross sections of a clothing surface . Although that method is effective for the purpose of recognizing the clothing state in the situation that the geometrical model of the clothing item is given in advance, the accuracy is insufficient when generally recognizing the shape without prior knowledge.

In the present paper, we propose a totally different method, which calculates geodesic distances more properly and formulates the flattening of the observed 3D surface as a problem of solving simultaneous equations given by the geodesic distances between the points on the surface. Section II explains a method of calculating the geodesic distance between two points on a surface using a 3D point cloud of the surface. Section III describes the formulation of the virtual flattening of a clothing surface using equations determined by the geodesic distances. Section IV describes methods of recognizing the

clothing item using the flattened view. After experimental results are presented in Section V, the results and future topics of research are discussed in Section VI.

II. CALCULATION OF GEODESIC DISTANCE

Although many methods of calculating the geodesic line using finite element meshes have been proposed [8][9], few studies have calculated a geodesic line from meshfree 3D data. Grossman et al. [10] proposed a voxel-based geodesic distance estimation method mainly for texture mapping. Both the mesh-based and the voxel-based methods assume uniformly dense 3D data of objects, that is not always kept in the case of 3D point clouds obtained by a range sensor or stereo cameras. In addition, the accuracy of those methods is limited in principle since they approximate the geodesic distances with a sequence of straight lines connecting adjacent triangle patches or voxels. For the calculation of a smooth geodesic line more directly from a 3D point cloud, the approach proposed by Kawashima et al. [11] that calculates geodesic lines in a meshfree way is effective. We follow their approach except for their method of obtaining a numerical solution .

A. Surface interpolation using the element-free Galerkin method (EFGM)

When analytically calculating geodesic lines of an arbitrary curved surface observed as a 3D point cloud, it is important to represent the surface with appropriate local approximation functions. Here, we represent the surface at $\boldsymbol{x} = (x, y)$ as $z(\boldsymbol{x})$ and obtain the local approximation functions at $\boldsymbol{x}$ using the EFGM[12]. With this approach, we can approximate the local surface function with continuous partial derivatives from a 3D point cloud in a meshfree manner. Specifically, $z(\boldsymbol{x})$ is approximated by a polynomial function comprising m terms. In a 2D domain, the polynomial basis vector can be, for example, $(1, x, y)(m = 3)$ or $(1, x, y, x^2, xy, y^2)(m = 6)$. We use $m = 3$ and thus have

$$z(\boldsymbol{x}) = \sum_{j=1}^{3} p_j(\boldsymbol{x})a_j(\boldsymbol{x}) = P^T(\boldsymbol{x})a(\boldsymbol{x}), \quad (1)$$

$$P^T(\boldsymbol{x}) = (1, x, y), a(\boldsymbol{x}) = (a_1(\boldsymbol{x}), a_2(\boldsymbol{x}), a_3(\boldsymbol{x}))^T.$$

The coefficient vector $a(\boldsymbol{x})$ is locally determined at each $\boldsymbol{x}$ using the moving least-squares approximation: $a(\boldsymbol{x})$ is determined by minimizing the weighted function

$$J = \sum_{l=1}^{N_{r0}} w(r_l)(z(\boldsymbol{x_l}) - z_l)^2, \quad (2)$$

$$r_l = |\boldsymbol{x} - \boldsymbol{x_l}|,$$

where $w(r)$ is a weight function defined by the distance between the target point, $\boldsymbol{x}$, and observed points $\boldsymbol{x_l}(l = 1, \cdots, N_{r0})$ within a fixed distance, r_0. In this study, a fourth-order spline function is used as the weight function following [11]:

$$w(r_l) = \begin{cases} 1 - 6\frac{r_l}{r_0}^2 + 8\frac{r_l}{r_0}^3 - 3\frac{r_l}{r_0}^4 & \text{if } 0 \leq r_l \leq r_0 \\ 0 & \text{if } r_0 < r_l \end{cases} . \quad (3)$$
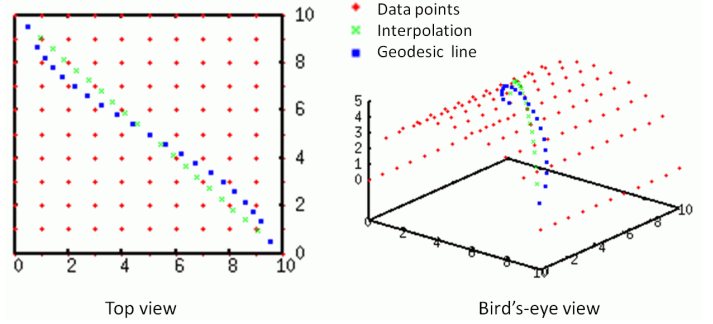

Fig. 1. Surface interpolation and geodesic line

The advantage of this formulation is that the depth and its first derivative can be continuously determined even when using the linear base function.

The depth and normal at $\boldsymbol{x}$ are calculated using the resultant $a(\boldsymbol{x})$:

$$z(\boldsymbol{x}) = a_1(\boldsymbol{x}) + a_2(\boldsymbol{x})x + a_3(\boldsymbol{x})y, \quad (4)$$

$$\boldsymbol{n}(\boldsymbol{x}) = (a_2(\boldsymbol{x})/D, a_3(\boldsymbol{x})/D, 1/D), \quad (5)$$

$$D = \sqrt{a_2(\boldsymbol{x})^2 + a_3(\boldsymbol{x})^2 + 1}.$$

The green points in Fig. 1 show an example of surface interpolation along the line $y = -x + 10$ using a 3D point cloud (red points) sampled from the surface of $z = \sqrt{25 - (x - 5)(x - 5)}$.

B. Numerical solution obtained using the zero-length spring analogy

To calculate the geodesic line between two points, P_s and P_e, we set M nodes on the surface to represent the line $P_s P_e = P_1 P_2 \ldots P_M$, where $P_s = P_1$, $P_e = P_M$ and $P_i = (x_i, y_i, z_i)$.

The problem of obtaining the geodesic distance of $P_s P_e$ can be set as minimizing L_{total} given by:

$$L_{total} = \sum_{i=1}^{M-1} L_i, \quad (6)$$

$$L_i = \sqrt{(x_{i+1} - x_i)^2 + (y_{i+1} - y_i)^2 + (z_{i+1} - z_i)^2}.$$

Because of the term including $z(\boldsymbol{x})$ determined by Eq. (4), L_{total} is a complex function. To stably solve the minimization, we make the zero-length spring analogy. Specifically, we assume that each segment $P_i P_{i+1}$ is a spring connecting two nodes, P_i and P_{i+1}, with a basis length (the length at neutral time) of zero and a spring constant k. The total length of all springs, L_{total}, is a minimum when the spring system comes into equilibrium.

Because each node is constrained to move on the surface, when a force $\boldsymbol{F}$ is exerted on a node, P_i, only the component of $\boldsymbol{F}$ along the surface, $\tilde{\boldsymbol{F}}$, affects the movement of P_i:

$$\tilde{\boldsymbol{F}} = \boldsymbol{F} - (\boldsymbol{F} \cdot \boldsymbol{n_i})\boldsymbol{n_i}, \quad (7)$$

where $\boldsymbol{n_i} = (n_{x_i}, n_{y_i}, n_{z_i})$ is a unit vector in the normal direction at P_i. Because the force exerted on P_i is only from two springs, the x component of $\tilde{\boldsymbol{F}}$ for P_i is

$$\tilde{F}_x = -k_{i-1}(1 - n_{x_i}^2)(x_i - x_{i-1})$$
$$+ k_i(1 + n_{x_i}^2)(x_{i+1} - x_i) + C_i, \qquad (8)$$
$$C_i = k_{i-1}n_{x_i}((y_i - y_{i-1})n_{y_i} + (z_i - z_{i-1})n_{z_i})$$
$$+ k_i n_{x_i}((y_{i+1} - y_i)n_{y_i} + (z_{i+1} - z_i)n_{z_i}).$$

Supposing P_i moves gently in a viscous fluid with a fluid coefficient γ, the equilibrium equation of the force in the x direction acting on P_i at time t is

$$\boldsymbol{A_i} \begin{pmatrix} x_{i-1} \\ x_i \\ x_{i+1} \end{pmatrix} + C_i + \gamma \frac{\delta x_i}{\delta t} = 0, \quad (9)$$
$$\boldsymbol{A_i} = \begin{pmatrix} k_{i-1}n_{a,i} & -k_{i-1}n_{a,i} - k_i n_{b,i} & k_i n_{b,i}, \end{pmatrix}$$
$$n_{a,i} = (1 - n_{x_i}^2), n_{b,i} = (1 + n_{x_i}^2).$$

Supposing γ is a large negative value, the points hardly move for $\Delta t = 1$; i.e., $C_{i,t} \simeq C_{i,t+1}$, $\boldsymbol{n_t} \simeq \boldsymbol{n_{t+1}}$. Hence, for all points, $P_i(i = 1, \cdots, M)$,

$$\boldsymbol{A_t x_{t+1}} + \boldsymbol{C_t} = -\gamma(\boldsymbol{x_{t+1}} - \boldsymbol{x_t}), \qquad (10)$$

where $\boldsymbol{x_t} = (x_{1,t}, x_{2,t}, \cdots, x_{M,t})^T$, $\boldsymbol{C_t} = (C_{1,t}, C_{2,t}, \cdots, C_{M,t})^T$, and $\boldsymbol{A_t}$ is a tridiagonal banded matrix. By applying the same analysis to the y direction, equations for one step of the successive approximation are obtained as

$$\boldsymbol{x_{t+1}} = (\boldsymbol{A_{x,t}} + \gamma \boldsymbol{I})^{-1}(\gamma \boldsymbol{x_t} - \boldsymbol{C_{x,t}}), \qquad (11)$$
$$\boldsymbol{y_{t+1}} = (\boldsymbol{A_{y,t}} + \gamma \boldsymbol{I})^{-1}(\gamma \boldsymbol{y_t} - \boldsymbol{C_{y,t}}). \qquad (12)$$

At each iteration, $\boldsymbol{z_{t+1}}$ and $\boldsymbol{n_{t+1}}$ are calculated using Eqs. (4) and (5) with $(\boldsymbol{x_{t+1}}, \boldsymbol{y_{t+1}})$.

The blue points in Fig. 1 show an example of the geodesic line obtained after the convergence of the successive approximation, using the green line as its initial position.

III. CALCULATION OF THE FLATTENED VIEW

A. Basic formulation

We assume that a clothing surface can be flattened onto a 2D plane, (u, v). Then, if we consider N points on the clothing surface, $P_i(x_i, y_i, z_i), i = 1, \cdots, N$, the flattening can be formulated as the problem of calculating the 2D coordinates of P_i on the plane when the surface is flattened, (u_i, v_i).

These coordinates should satisfy the equation

$$\sqrt{(u_i - u_j)^2 + (v_i - v_j)^2} = G_{i,j}, \qquad (13)$$

where $G_{i,j}$ is the geodesic distance between P_i and P_j on the surface.

Although the number of equations of the form of Eq. (13) is $_NC_2$ if we consider all combinations of N points, not all are necessarily required as long as the number of equations related to one point is more than two, which is the number of
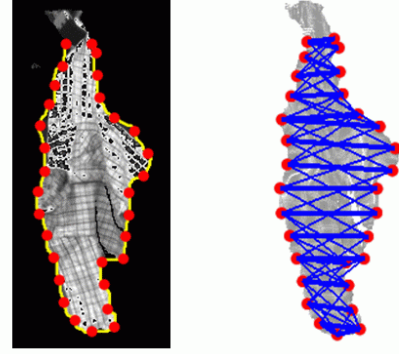
Fig. 2. Point pairs for calculating geodesic distances

unknowns for the point. By representing the use/disuse of $G_{i,j}$ as $B(i,j) = \{1, 0\}$, the flattening becomes the minimization problem of the equation

$$H(\boldsymbol{u}, \boldsymbol{v}) =$$
$$\sum_{i=1}^{N-1} \sum_{j=i+1}^{N} B(i,j)(\sqrt{(u_i - u_j)^2 + (v_i - v_j)^2} - G_{i,j})^2.$$
$$(14)$$

The solution is then obtained by solving $2N$ simultaneous equations, where the two equations for each P_i are

$$\frac{\partial H(\boldsymbol{u}, \boldsymbol{v})}{\partial u_i} = 0, \frac{\partial H(\boldsymbol{u}, \boldsymbol{v})}{\partial v_i} = 0.$$

B. Problem setting for clothing

As noted in Section I, the present paper assumes that almost all of one side of a clothing item is observed when the item is held by a robot hand in the air. We then choose points from the boundary of the observed clothing region, $P_i(x_i, y_i, z_i), i = 1, \cdots, N_b$, as shown by red points in Fig. 2.

Before considering the constraints regarding geodesic distances, the conditions related to the neighboring points, P_{i_n} for P_i, are introduced to keep the local shape:

$$\sqrt{(u_i - u_{i_n})^2 + (v_i - v_{i_n})^2} = E_{i,i_n}, \qquad (15)$$
$$E_{i,i_n} = \sqrt{(x_i - x_{i_n})^2 + (y_i - y_{i_n})^2 + (z_i - z_{i_n})^2},$$
$$i_n = \{i - 2, i - 1, i + 1, i + 2\}.$$

Because the gravity force pulls the item in the vertical direction, folds on the surface occur mainly in the horizontal direction. We thus select point pairs for calculating the geodesic distance such that the points of a pair have similar height; the points that have the closest height, $P_{i_{h0}}$, are selected as the pair P_i as shown by thick blue lines in Fig. 2. Points close to $P_{i_{h0}}$ are then used for additional pairs as shown by thin blue lines.

Then, $(\boldsymbol{u}, \boldsymbol{v})$, which satisfy Eq. (15) and

$$\sqrt{(u_i - u_{i_h})^2 + (v_i - v_{i_h})^2} = G_{i,i_h} \qquad (16)$$
$$i_h = \{i_{h0}, i_{h0} \pm id\}$$

in accordance with least-square-error standards are obtained by the minimization of $H'(\boldsymbol{u}, \boldsymbol{v})$:

$$H'(\boldsymbol{u}, \boldsymbol{v}) =$$
$$\sum_{i=1}^{N_b} (\sqrt{(u_i - u_{i_n})^2 + (v_i - v_{i_n})^2} - E_{i,i_n})^2$$
$$+ \sum_{i=1}^{N_b} (\sqrt{(u_i - u_{i_h})^2 + (v_i - v_{i_h})^2} - G_{i,i_h})^2. \qquad (17)$$

In the experiments reported in the present paper, $N_b = 30$ and $id = 2$ are used.

IV. RECOGNITION USING THE FLATTENED VIEW

Because the shape of the flattened view is hardly affected by physical deformation, it should be useful for various recognitions, such as the classification of the clothing category. For the classification, we represent the common model of each category using likelihood images, $I(i, j)$, in a manner similar to that employed by Hue et al.[4]. Figure 3 (a) shows the concept of likelihood images. Each pixel of the likelihood image represents the possibility of the boundary of the flattened shape of each category. By combining typical shapes of the same category into one image or using statistical models such as the active shape model[13], likelihood images that represent within-class shape variation due to different designs are available.

When classifying the flattened view of an observed item using the likelihood images, the size of the view is normalized using the vertical length, and the contour of the view is then set on each likelihood image so that the holding position coincides with the likelihood image. The consistency between the contour and the likelihood image of each category is simply measured using R:

$$R = \frac{\sum_{n=1}^{N_c} I(i_n, j_n)}{N_c}, \qquad (18)$$

where N_c is the number of pixels of the contour and (i_n, j_n) denotes the coordinates of contour point $n(n = 1, \cdots, N_c)$ on the image. The category having the highest R is selected.

For the automatic handling of a clothing item by a robot, the positions of important parts, such as the corners of the bottom, are also essential information. The flattened view is also useful for obtaining such information. Similarly to how the whole shape was considered, we store the possibility of each part in a likelihood image. To this end, at the same time that the likelihood image of the whole shape is made, the distribution of each important part is also recorded in a different layer of a multilayer likelihood image of each category. In the case of Fig. 3(b), the likelihoods of the bottom-corner layer and armpit layer are superposed on the whole-shape likelihood
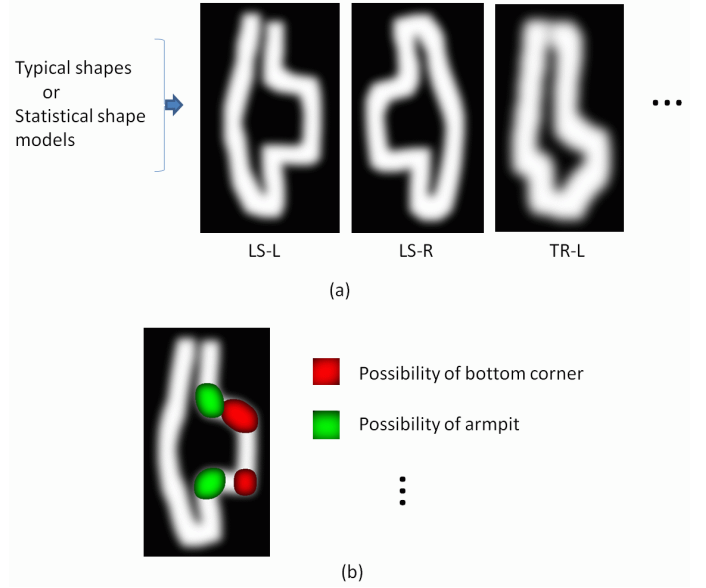

Fig. 3. Likelihood images for recognition: (a) likelihood images of each category; (b) concept of a multilayer likelihood image.

image using red and green respectively. Once an observed item is classified into a category using the whole-shape layer likelihood image, other layers for important parts are referred to so as to detect the parts by searching for the characteristic features of each important part only in the area with high possibility (e.g., the red part for bottom corners). As such points are found on the flattened view, the 3D positions of the parts also become known in the 3D observation data via the view.

V. EXPERIMENTS

A. Geodesic distance on measured surface

To examine the accuracy of geodesic lines on actually measured surface, a piece of paper with a line drawn on it (Fig. 4(a)) was deformed and measured using a trinocular stereo camera[14]. On each depth image of the observed surface (Fig. 4(b)), the 2D coordinates corresponding to the points S and E in Fig. 4(a) were manually given. The 3D coordinates of the points were read from the depth image and used as the start and end points for calculating the geodesic line. Fig. 4(c)(d) show the geodesic lines (D and C in Table 1) obtained by the method described in Section II, where grey dots in the middle and right images represent observed 3D points. The green points show the surface interpolation along the straight line connecting S and E on the depth image, while the red points show the resultant geodesic lines using the green points as the initial lines. Table 1 shows the results of five different deformations. In three cases (A, B and D in Table1), the geodesic lines got close to the drawn line and the difference in length from the actual value, 200 mm, was less than 2.1 mm. In the two remaining cases, calculated geodesic lines partially deviated
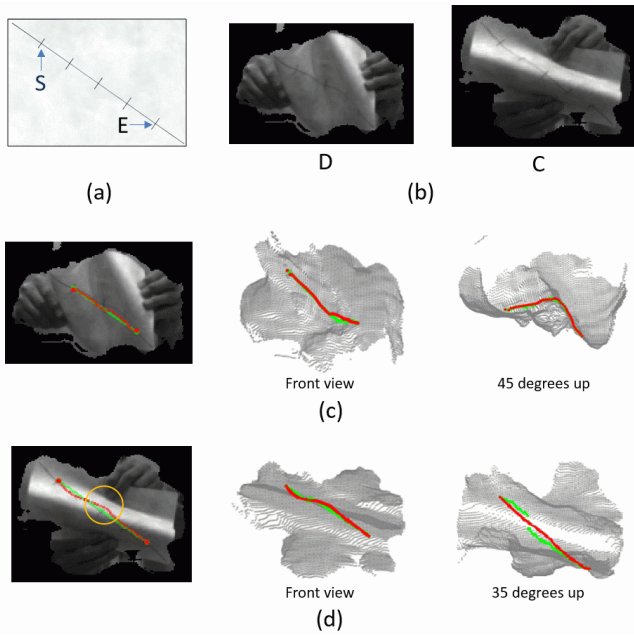
Fig. 4. Experiment 1: Geodesic distance on measured surface: (a) Paper used in the experiment; (b) observed 3D data (D, C); (c) geodesic line of D; (d) geodesic line of C.

Table 1   Accuracy of geodesic lines on measured range data

Data	A	B	C	D	E
Length of initial line (mm)	215.5	217.4	236.4	219.0	241.7
Length of geodesic line (mm)	200.1	202.1	209.1	200.6	207.4
Error rate (%)	0.05	1.1	4.6	0.3	3.7

from the drawn line as marked by a orange circle in Fig, 4(d) and the length errors were about 7 mm and 9 mm. These deviations occurred around the part where the 3D data of the surface is lacked as we can see a white gap in the 35 degrees up view of Fig. 4(d). From these results, we estimate the error of the geodesic line as around 1% without observation lacking along the line, while 5% for the case with the lack.

B. Flattened view of 3D observation data

Experiments were conducted using three observation data sets for long-sleeve shirts and three observation data sets for trousers. Since these items are easily held at the tip of a sleeve or leg by grasping the lowest part after picking up them placed in an arbitrary shape (e.g., [4]) , we used observations for such situations. For the experiments, after taking 3D data from different directions, the 3D data for which almost all one side of an item is observed were manually selected. Figure 5(a) shows an example of the flattening process in the case of a long-sleeve shirt. The red lines in Fig. 5 show geodesic lines calculated using the method described in Section II. The blue line shows the resultant flattened view obtained using the method described in Section III. The view was globally well obtained, although parts around the armpits were not produced because points around the armpit were not detected owing to
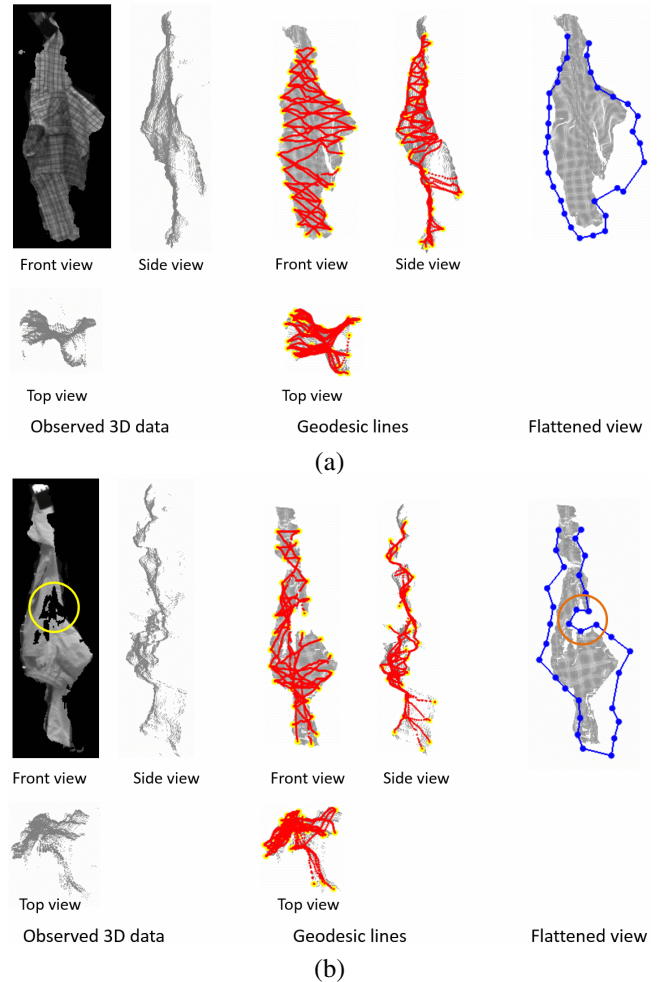

Fig. 5. Flattening of 3D observation data

the occlusion of the part. To avoid such situations, observations need to be made from different directions.

In the case of trousers, because one leg is folded when the trousers are held at the tip of the other leg, it is almost impossible to find 3D data including all of one side of the item. Instead, in the experiments of this paper, we consider the flattened view of the item after one leg is folded as shown in Fig. 5(b). In this example, 3D observation data for the part of the upper leg marked by the yellow circle in the figure was largely lacking. As a result, some boundary points of the observed clothing region correspond to points inside the leg. This fact was reflected in the flattened view, as marked by the orange circle. The zigzag contour of the uppermost part was due to the twisting of the part in the real world. The magnitude of this flaw should be lessened if we use the 3D data of observations made from the direction perpendicular to the normal of the part.

C. Classification

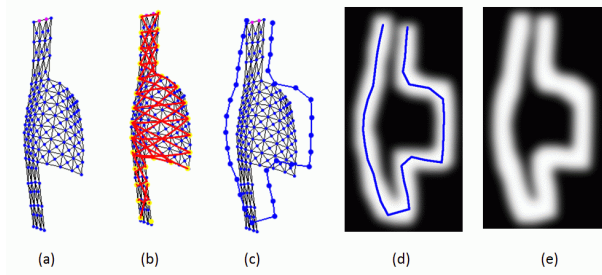Using the resultant flattened views, we also conducted preliminary experiments on category classification. Although,
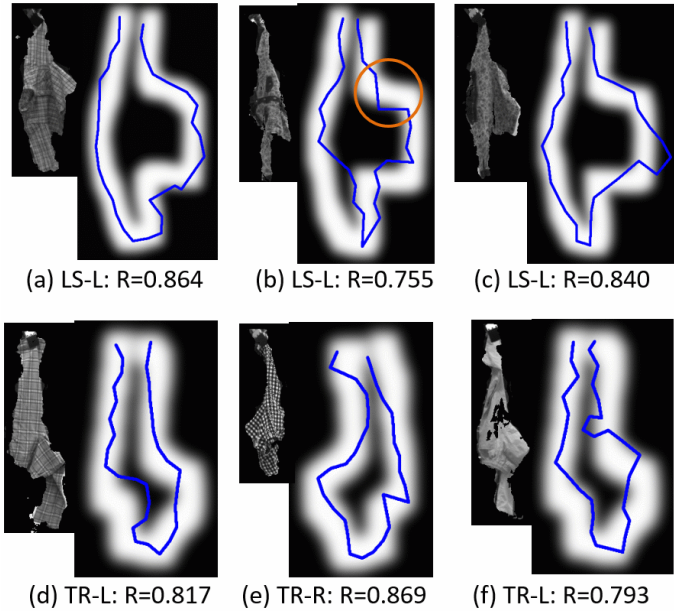
Fig. 6. Process of building a model likelihood image

(a) LS-L: R=0.864   (b) LS-L: R=0.755   (c) LS-L: R=0.840

(d) TR-L: R=0.817   (e) TR-R: R=0.869   (f) TR-L: R=0.793

Fig. 7. Recognition using the flattened view

Fig. 8. Preliminary trial of detecting important parts

as noted in Section IV, a common model should be built to absorb the shape variation within the same category, this time, common models that have been calculated from one typical shape model of each category were temporarily used. Figure 6 shows the process of creating the likelihood image. After one clothing model with a typical shape of one category was selected, the shape when the clothing is held at the tip of a sleeve or leg was simulated using Maya [15](Fig. 6(a)). The flattened view of the simulated 3D shape was calculated using the proposed method as shown in Fig. 6(c) using the geodesic distances (red lines in Fig. 6(b)). To absorb the size and design variation of each category, the resultant contour is expanded and then smoothed using a Gaussian function. Figure 6(e) shows the likelihood image for a long-sleeve shirt that faces left (LS-L). In addition to this example, the likelihood images of a long-sleeve shirt that faces right (LS-R), trousers that face left (TR-L) and trousers that face right (TR-R) were prepared.

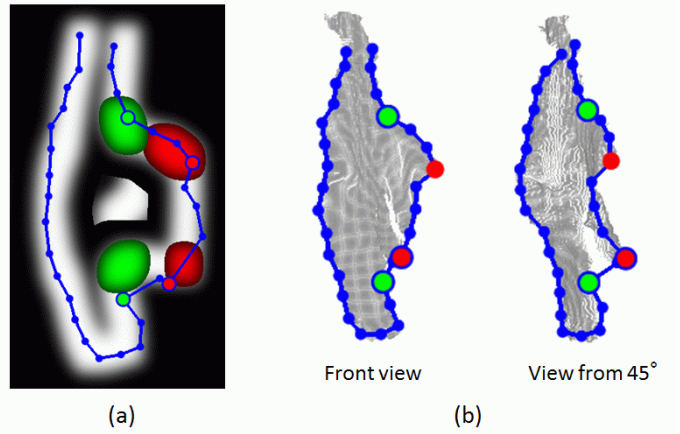The flattened views of six observation data sets were clas-

sified by setting the contours of the views on each likelihood image at the holding position after normalizing the size using the vertical length of the flattened view. Because the holding position slightly changes depending on how the robot hand grasped the item, the highest consistency R obtained while moving the contour horizontally on the image was used. Figure 7 shows the results for all six flattened views on the likelihood image that gives the highest consistency. In the case of Fig. 7(b), a part around one bottom corner was not seen in the observation data. As a result, boundary points around the part were inside the body. This situation manifests as the convex region marked by the orange circle. Again, the twisting of legs and sleeves in the real world adversely affected the results for some parts of the clothing. Despite these partial errors, all flattened views were correctly classified.

Using the result of Fig. 7(a), a trial of detecting important parts was performed as shown in Fig. 8. The points that have a characteristic feature in the high-possibility region of the likelihood image of each important layer were detected in the flattened view: convex points for bottom corners and concave points for armpits. Large red and green points in Fig. 8(a) show the detected points. Then, by re-projecting the points to the original observed 3D data, these characteristic points were detected as shown in Fig. 8(b).

VI. CONCLUSION

We proposed a method of virtually flattening a clothing surface on a 2D plane using an observed 3D point cloud. To this end, a method of stably calculating the geodesic distance between two points on the surface was proposed. Surface interpolation using the EFGM and a numerical solution based on a zero-length spring analogy allow the proposed method to work well in practice even when the observation data are lacking or have an uneven point distribution as shown in our first experiment.

Because geodesic distances between surface points are 2D distances of the points in the flattened view, the proposed method calculates the view by solving simultaneous equations given by the geodesic distances. In our second experiment, the flattened views were globally well obtained, although there were partial errors due to occlusions in the observed 3D data.

The obtained flattened view is useful for the recognition of observed items. In our third experiment, we showed that the views are effective for classification of the clothing category. In addition, a preliminary trial on the detection of important parts of clothing demonstrated the good prospects of using the flattened view as a mediator between common models and items having a deformed shape.

Although we used 3D data of observations made from one viewing direction in this paper, the experimental results indicate the necessity of using data of several observations made from different viewing directions to accurately flatten one whole side. However, because the clothing item may be partially deformed when rotated for observation from different directions, it is another challenging subject to integrate sets of 3D data of observations made at different times. We expect that flattened views will also be useful in solving this problem.

ACKNOWLEDGMENT

REFERENCES

[1] Y. Kita, F. Kanehiro, T. Ueshiba and N. Kita: "Strategy for Folding Clothing on the Basis of Deformable Models", In *Proc. of International Conference on Image Analysis and Recognition 2014*, pp.442–452, 2014.

[2] Y. Li, C.F. Chen, and P.K. Allen: "Recognition of Deformable Object Category and Pose", In *International Conference in Robotics and Automation (ICRA) 2014*, pp.5558–5564, 2014.

[3] F. Osawa, H. Seki, and Y. Kamiya: "Unfolding of massive laundry and classification types by dual manipulator", *Journal of Advanced Computational Intelligence and Intelligent Informatics*, Vol. 11, No.5, 457–463, 2007.

[4] J. Hu and Y. Kita: "Classification of the category of clothing item after bringing it into limited shapes", In *Proc. of International Conference on Humanoid Robots 2015*, pp.588–594, 2015.

[5] D. Triantafyllou, I. Mariolis, A. Kargakos, S. Malassiotis and N. Aspragathos: "A geometric approach to robotic unfolding of garments", *Robotics and Autonomous Systems*, Vol 75, pp. 233–243, 2016.

[6] A. Doumanoglou, A. Kargakos, T-K Kim, S. Malassiotis: "Autonomous Active Recognition and Unfolding of Clothes using Random Decision Forests and Probabilistic Planning", In *International Conference in Robotics and Automation (ICRA) 2014*, pp.987–993, 2014.

[7] Y. Kita, T. Ueshiba, F. Kanehiro and N. Kita: "Recognizing clothing states using 3D data observed from multiple directions", In *Proc. of International Conference on Humanoid Robots 2013*, pp.227–233, 2013.

[8] P. Bose, A. Maheshwari, C. Shu, and S. Wuhrer: "A survey of geodesic paths on 3D surfaces", *Computational Geometry*, Vol 44, pp. 486–498, 2011.

[9] Y. Zhong and B. Xu: "A physically based method for triangulated surface flattening", *Computer-Aided Design*, Vol. 38, pp. 1062–1073, 2006.

[10] R. Grossmann, N. Kiryati, and R. Kimme: "Computational Surface Flattening: A Voxel-Based Approach", *IEEE Trans. on Pattern Anal. and Machine Intelli.*, vol. 24, no.4, pp.433–441, 2002.

[11] T. Kawashima, S. Yabashi, H.Noguchi, K. Yokohori: "Meshless Method for Searching Geodesic Line by using Moving Least Squares Interpolation", In *Research Report on Membrane Structures*, pp. 1–6, 1999.

[12] T. Belytschko, Y. Y. Lu and L. Gu: "Element-free Galerkin methods", *International Journal for Numerical Methods in Engineering*, Vol 37, No. 2, pp. 229–256, 1994.

[13] T.F. Cootes, C.J. Taylor, D.H. Cooper and J. Graham: "Active shape models - their training and application", *Computer Vision and Image Understanding*, Vol 61, No. 1, pp. 38–59, 1995.

[14] T. Ueshiba: "An Efficient Implementation Technique of Bidirectional Matching for Real-time Trinocular Stereo Vision", In *Proc. of 18th Int. Conf. on Pattern Recognition*, pp.1076–1079, 2006.

[15] D. A. D. GOULD: *"Complete Maya Programming"*, Morgan Kaufmann Pub, 2004.